Interplanetary Coronal Mass Ejections as the Driver of Non-recurrent Forbush Decreases

Athanasios Papaioannou[1] , Anatoly Belov[2] , Maria Abunina[2] , Eugenia Eroshenko[2] , Artem Abunin[2] ,
Anastasios Anastasiadis[1] , Spiros Patsourakos[3] , and Helen Mavromichalaki[4]

[1] Institute for Astronomy, Astrophysics, Space Applications and Remote Sensing (IAASARS), National Observatory of Athens I. Metaxa & Vas. Pavlou St., 15236 Penteli, Greece; atpapaio@astro.noa.gr

[2] Institute of Terrestrial Magnetism, Ionosphere and Radiowave Propagation by N.V. Pushkov RAS (IZMIRAN), Moscow Troitsk, Russia

[3] Section of Astrogeophysics, Department of Physics, University of Ioannina, 45110 Ioannina, Greece

[4] Faculty of Physics, National and Kapodistrian University of Athens, 15784 Athens, Greece

Abstract

Interplanetary coronal mass ejections (ICMEs) are the counterparts of coronal mass ejections (CMEs) that extend in the interplanetary (IP) space and interact with the underlying solar wind (SW). ICMEs and their corresponding shocks can sweep out galactic cosmic rays (GCRs) and thus modulate their intensity, resulting in non-recurrent Forbush decreases (FDs). In this work, we selected all FDs that were associated with a sudden storm commencement (SSC) at Earth, and a solar driver (e.g., CME) was clearly identified as the ICME's source. We introduce and employ the t_H parameter, which is the time delay (in hours) of the maximum strength of the interplanetary magnetic field from the FD onset (as is marked via the SSC), and consequently derive three groups of FD events (i.e., the early, medium, and late ones). For each of these we examine the mean characteristics of the FDs and the associated IP variations per group, as well as the resulting correlations. In addition, we demonstrate the outputs of a superposed epoch analysis, which led to an average time profile of the resulting FDs and the corresponding IP variations, per group. Finally, we interpret our results based on the theoretical expectations for the FD phenomenon. We find that both the shock sheath and the ejecta are necessary for deep GCR depressions and that the FD amplitude ($A0$) is larger for faster-propagating ICMEs. Additionally, we note the importance of the turbulent shock-sheath region across all groups. Finally, we present empirical relations connecting $A0$ to SW properties.

Unified Astronomy Thesaurus concepts: Solar coronal mass ejections (310); Galactic cosmic rays (567); Solar wind (1534)

1. Introduction

A solar eruptive event, such as a coronal mass ejection (CME), results in the ejection of plasma and frozen-in magnetic field into the interplanetary (IP) space (Schwenn et al. 2006). As the interplanetary counterparts of CMEs (e.g., interplanetary coronal mass ejections [ICMEs]) propagate outward from the Sun, they overtake the underlying solar wind (SW), leading to a sheath of compressed plasma at the front of the ICME. Additionally, if the CME/ICME is faster than the local Alfvén speed, a shock will be formed (Forsyth et al. 2006). Galactic cosmic rays (GCRs) are high-energy charged particles that are accelerated outside our solar system and are omnipresent within the heliosphere. Hence, during their propagation, ICMEs fill large parts of the innermost heliosphere and modulate the flux of GCRs at Earth (Barnden 1973; Belov et al. 2001; Papaioannou et al. 2010; Dumbović et al. 2011, 2012; Jordan et al. 2011), Mars (Freiherr von Forstner et al. 2018; Guo et al. 2018; Papaioannou et al. 2019), and beyond (Witasse et al. 2017; Winslow et al. 2018), leading to short-term intensity depressions known as Forbush decreases (FDs; Forbush 1938; Cane 2000; Belov 2009).

A lot of work has focused on the quantification of the influence of the ICME structures on the properties of FDs (Lockwood 1971; Dumbović et al. 2011; Richardson & Cane 2011; Abunin et al. 2012; Abunina et al. 2013; Belov et al. 2014, 2015). Our current theoretical understanding is that there are two basic processes that contribute to the observed FDs: (i) variations in the turbulent

sheath region that leads to decreases of the GCRs' radial diffusion coefficient (Barnden 1973; Belov et al. 1976; Wibberenz et al. 1998), and (ii) a local decrease in the GCRs' intensity driven by the (at least partially) closed field line geometry of the magnetized ejecta of ICMEs that occurs as the ICME moves over the observing point (Cane 2000; Krittinatham & Ruffolo 2009; Richardson & Cane 2011). As a result, two-step FDs are marked (Barnden 1973). Such FDs refer to a prime subset of GCR decreases for an observer (e.g., Earth) with a trajectory that crosses both the shock and the magnetized ejecta of an ICME (Cane 2000; Belov 2009; Jordan et al. 2011). At the same time, the majority of the observed (i.e., registered) FDs are one-step FDs. These result either from the effect of only a shock or from the effect of the ejecta. Therefore, the simplest grouping of ICME disturbances that affect GCRs is (1) only ejecta, (2) only shock, and (3) shock, sheath, and ejecta. Therefore, the relative position of the observer to the propagating disturbance holds a prominent role in the resulting FD. One should further note that CMEs originating outside heliolongitudes of $\Phi_s = \pm 50°$ from the Sun's central meridian can preferentially give ground to FDs of category 2 (Cane et al. 1996), since the observer—in this case— only encounters the flanks of the shock. Additionally, the driving CME/ICME should be energetic enough in order to produce a strong shock that will lead to a short-term GCR depression (Dumbović et al. 2011).

It should also be mentioned that a much larger diversity is identified in the recorded time profiles of FDs. This is due to the following: (i) A subset of ICMEs are magnetic clouds

(MCs), which are characterized by a strong magnetic field (B) and a smooth rotation of its vector components, typical of a so-called flux-rope (Burlaga et al. 1982; Burlaga 1991). Such ICMEs/MCs have proved to be very effective in the production of FDs (Richardson & Cane 2011; Belov et al. 2015; Masías-Meza et al. 2016). (ii) ICMEs interact with the underlying SW and other propagating interplanetary disturbances (e.g., other ICMEs, Lugaz & Farrugia 2014; Winslow et al. 2018; and high-speed streams [HSSs] from coronal holes). As a result, the theoretically expected (one- or two-step) structure of FDs is usually masked. Therefore, subsequent complications in the classification of FDs are ever present in the actual recorded FD time profiles. Hence, in order to pursue an objective (as possible) classification of actual FD events, the selection/grouping of the events should be based on an objective quantitative parameter.

In this work, we first group FD events in three different groups based on the criterion of the time delay (in hours) from the time of the maximum magnetic field strength of the interplanetary magnetic field (IMF) ($t_{B_{max}}$) in the FD to the onset of the FD event (as is marked via the sudden storm commencement [SSC], t_{SSC}), i.e., t_H (in hours). The argumentation, in favor of the selection of this parameter, is that the dominant IP characteristic for a charged particle (i.e., GCRs) is the magnetic field. Therefore, the maximum intensity of the IMF is an objective classifier. Evidently, there are cases in which this maximum is at the start of the event (e.g., clean shock wave cases) or shifted farther into the disturbance (e.g., sheath or ejecta/MC). As we will show, later on, from the distribution of t_H with respect to the solar longitude of the agent CME/ICME, it was possible to identify only four cases that could be identified as shock-only (category 2) events. As a result, we utilized the parameter t_H, while restricting our sample within $-30° \leqslant \Phi_s \leqslant 30°$, and thus focusing on category 3 events (Cane et al. 1996). The goal of this work is to quantify the effect of ICMEs on GCRs and in particular their ability to lead to FDs. Additionally, we characterize the mean properties of FDs and ICMEs at 1 au for each group, applying a superposed epoch analysis (SEA) on the in situ plasma data and the corresponding FDs at a fixed rigidity of 10 GV recorded at Earth by the worldwide neutron monitor (NM) network (Belov et al. 2015). This statistical method provides the averaged (e.g., mean) properties per group of events and offers a common base for comparisons. Such a study has been applied to the properties (e.g., magnetic field and plasma parameters) of MCs (Lepping et al. 2003), to the effect of corotating interaction regions and ICMEs to GCRs (Badruddin 2016), and to the effect of ICMEs with MCs on GCR decreases (Masías-Meza et al. 2016).

Our work is a natural continuation of the former studies, with a clear addition toward the identification of all interplanetary structures (ICMEs, SW) that lead to noticeable GCR decreases and the quantification of their efficiency in modulating the GCRs as is demonstrated by the FD mean characteristics per group. That said, we present a systematic quantification of the dependence of critical FD timing parameters and FD characteristics (i.e., magnitude, anisotropy) on numerous ICME and SW variables, and we also provide expected time profiles, aiming at establishing empirical relations that shed light on the FD phenomenon.

2. Analysis

2.1. Data Used

Data on FDs and IP disturbances have been compiled into a database (Forbush Effects and Interplanetary Disturbances—FEID[5]) by the IZMIRAN Cosmic Ray Group. It includes hourly data from the worldwide network of NMs from 1957 (when continuous observations began) up to the present—calculated by the Global Survey Method (GSM; Belov et al. 2018)—taking into account the unique properties of each station such as coupling coefficients, asymptotic directions, and yield functions (Asipenka et al. 2009); *GOES* measurements (continuously updated; 5 minutes); the OMNI database hourly IP data; the list of SSCs from ftp://ftp.ngdc.noaa.gov/STP/SOLAR_DATA/SUDDEN_COMMENCEMENTS/ and solar flares reported in the solar geophysical data.[6] The FD database also includes all relevant IP data and geomagnetic indices (Kp, Dst). In order to pinpoint the characteristics of the recorded FDs (e.g., magnitude, decrement, 3D anisotropy), we use the results of GSM (Belov et al. 2018).

FEID includes more than 7000 FDs, and thus for any study on FDs a sufficiently large sample of events should, in principle, be retrieved. However, we limited the study to the time period between 1996 and 2017, aiming at a complete parametric grid. Furthermore, in order to get a clean sample for the purposes of this work, we restricted ourselves to events in which the following occurred:

1. An interplanetary shock wave was observed near Earth, causing a sudden storm SSC. As a result, 1515/>7000 events were identified in FEID.
2. ICMEs and IMF data were complete. This is because not all of the 1515 FDs were associated with ICMEs, since several were due to HSSs and thus were not suitable for this study. Moreover, FD events for which there were no measurements of the IMF (e.g., all the FD events of the 19th Solar Cycle), or for which such measurements were incomplete, were excluded. As a result, a sample of 272 events that we related to an ICME (with reasonable confidence) was identified.
3. Solar sources were identified. In particular, since we wanted to inspect the relevant distribution of the FD events with respect to the heliolongitude of their solar source (see Section 3), we further limited our sample to 173/272.

Finally, it was necessary to exclude from the analysis events that were (i) caused by more than one source and (ii) subsequent events (i.e., events that occurred in close time succession). As a result, our initial sample consisted of 65 well-identified, isolated events, representative of FDs related to ICMEs with identified solar drivers (e.g., CME, solar flare).

2.2. An Example Event

Before we proceed, we provide here (see Figure 1) an example of one event, at 2002 April 17–20, that illustrates the way that GCRs and IP data are combined in the vicinity of a shock and an ICME/MC in order to demonstrate how GCRs respond to the passage of these structures, resulting in the FD. Please note that this is a two-step FD (Cane 2000).
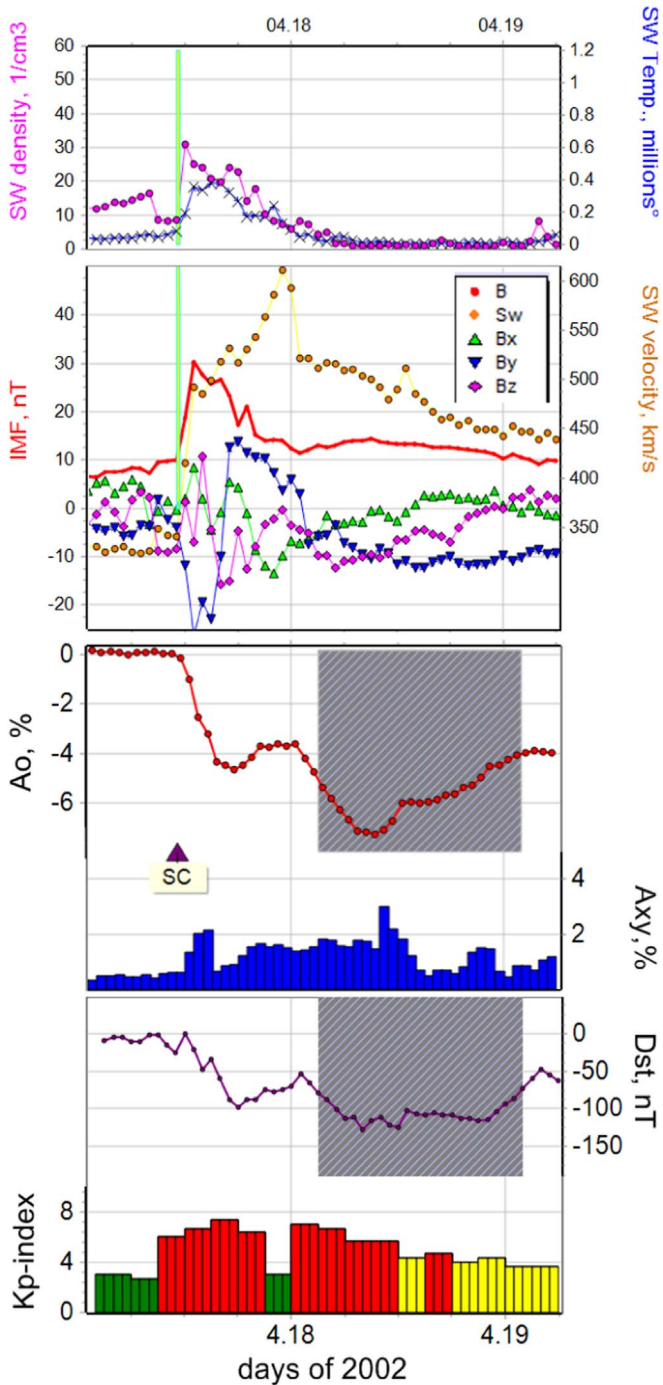
Figure 1. Observations of the passage of an ICME from Earth and the resulting FD, during 2002 April 17–20. The panels display, from top to bottom, SW proton temperature and density [cm^{-3}]; SW speed and the IMF intensity (in red) [nT], together with its components; GCR variations at a fixed rigidity of 10 GV, $A0$ [%]; anisotropy of GCRs, A_{xy} [%]; Dst [nT]; and Kp. The shaded area depicts the start and end times of the MC as is identified in the list of Cane & Richardson (http://www.srl.caltech.edu/ACE/ASC/DATA/level3/icmetable2.htm); the vertical line presents the arrival of the upstream shock with the identification of an SSC.

The shock is denoted with a blue vertical line and a legend of "SSC." The SW observations in Figure 1 are from the *Advanced Composition Explorer*/Solar Wind Electron, Proton, and Alpha Monitor (McComas et al. 1998). A strong enhancement in the total magnetic field *B* (second panel from the top; red line) is marked, leading to $B_{max} = 30$ nT. After the

shock, a sheath region follows, lasting for ~14 hr. Finally, an MC arrives—denoted as a gray shaded rectangle in the panels of the plot. As a result, the recordings of NMs show a clear depression that stems from the shock and extends into the sheath region, which constitutes the first step of the FD. Then, a second decrease (i.e., the second step) commences upon the entry into the ICME/MC, reaches maximum depression almost at the start of the MC, and then the recorded flux at NMs starts to recover. We note that the smooth recovery phase is briefly interrupted at around midday on April 18. This interruption is associated with a brief (in terms of duration) spike-like jump of the SW speed with no other clear characteristic in the in situ measurements. Therefore, this effect is most probably attributed to an internal feature of the particular MC, driven by one agent CME–ICME (Patsourakos et al. 2016). The total decrease of GCRs from the passage of the shock to the minimum inside the MC is 7.2% for 10 GV particles. At the same time, the Dst index reaches a first minimum of −100 nT that coincides with the first step of the FD and its minimum (−125 nT) in accordance with the second step (e.g., while in the MC). The Kp index shows a similar behavior (bottom panel of Figure 1).

For each FD event recorded we provided our own associations, trying to identify the corresponding solar source and, when possible, the related causative CME. For this purpose, we utilized the catalog of CMEs (Gopalswamy et al. 2009b) based on recordings from the Large Angle and Spectrometric Coronagraph (LASCO; Brueckner et al. 1995) on board the *Solar and Heliospheric Observatory* (*SOHO*; Domingo, Fleck, and Poland, 1995), available at https://cdaw.gsfc.nasa.gov/CME_list/, and the ICME simulations from the Wang–Sheeley–Arge ENLIL cone model that supplies the predicted arrival time of a heliospheric disturbance to 1 au (Arge & Pizzo 2000), available at https://iswa.gsfc.nasa.gov/IswaSystemWebApp/. Additionally, we used context data from the *Solar Dynamics Observatory*/Atmospheric Imaging Assembly in order to identify significant events (e.g., solar flares, dimmings; Lemen et al. 2012) and, when available, observations from the coronagraphs on board the *Solar TErrestrial RElations Observatory* (Howard et al. 2008). As a result, we were led to a single parent solar source identification per FD event or multiple ones, which were then cross-validated with the Richardson and Cane ICME list available at http://www.srl.caltech.edu/ACE/ASC/DATA/level3/icmetable2.htm, a published list of halo CMEs (Michalek et al. 2006) and a list of 99 MCs (Gopalswamy et al. 2008, 2009a). In particular, we calculated and/or tabulated the following quantities:

1. FD magnitude [in%];
2. 3D anisotropy [A_{xy}, in %; A_z, in %];
3. in situ measurements of the ICME;
4. parent solar event characteristics (e.g., CME and solar flare);
5. resulting geomagnetic indices (i.e., Kp_{max}, Ap_{max}, Dst_{min}).

We also include a quality index for the solar association(s), ranging from 1 to 5, based on the evaluation of the identified relation. The higher the number (i.e., 5), the more concrete the association. The purpose of such an index is to provide a quantification on the estimations made during the identification of the solar sources. Naturally, there are both straightforward and complex cases. This index (as any other one) provides different levels of such an evaluation and is subjective. Every
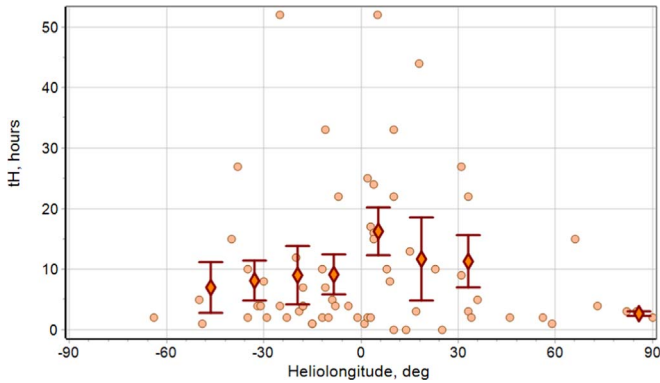
Figure 2. Time delay t_H of the achieved maximum IMF intensity with respect to the onset of the FD (SSC) vs. the heliolongitude of the apparent source (flare) of the agent CME; the diamonds with the error bars present the mean values per longitudinal intervals of 15°.

effort has been made in order to identify the most likely situation as concerns the driving solar sources.

3. Results and Discussion

3.1. Time of the Peak IMF Intensity and the Heliolongitude of the Sources

Figure 2 depicts the distribution of the t_H parameter, which is the time delay (in hours) from the time of maximum of the magnetic field strength of the IMF in the FD to the onset time of the FD event (as denoted by the SSC), with respect to the heliolongitude Φ_s of the parent solar event (e.g., solar flare associated with the CME/ICME driving the resulting FD). The largest values of t_H (e.g. ∼50 hr) are associated with solar sources located within the central part of the visible solar disk (i.e., $-40° \leqslant \Phi_s \leqslant 40°$), and the spread of the values is large (from practically 0 to 50 hr). However, for longitudes closer to the limb (e.g., east, $\Phi_s < -40°$, or west, $\Phi_s > 40°$) all t_H resulting values fall under ∼10 hr. Therefore, it seems that for these limb events, the maximum of the IMF is closer to the initiation of the FD.

A valid assumption is that such limb events fall mostly under category 2 (see Section 1; with an interplanetary shock, alone, driving the FD). We have further checked all of the events presented in Figure 2, making stack plots (similar to Figure 1) for each case. For the limb events, it seems that there is only one semi-exception: the event on 2000 October 28 ($t_H =$ 15 hr). In this particular case, both a shock and an MC were spotted (Richardson & Cane 2010). However, our assessment of the event suggests that it is probable that there are two solar sources involved, so that the shock and the MC are most likely related to different sources. Next, an attempt to retrieve a sample of clean shock-related FDs for the east and west bins, respectively, took place. It turned out that such a selection was very difficult to apply—especially for FDs related to eastern sources. Many events from those that could be candidates for category 1 (only shock) were not included in the selected events, because either there were doubts about the quality of the solar associations (i.e., not clear cases) or signs of ejecta were evident in the in situ plasma data. As a result, there were only four events that would fall under this category (i.e., only shock; see Section 1):

1. Event 1 at 1998 April 23 on 18:25 UT.
2. Event 2 at 1998 October 23 on 12:30 UT.
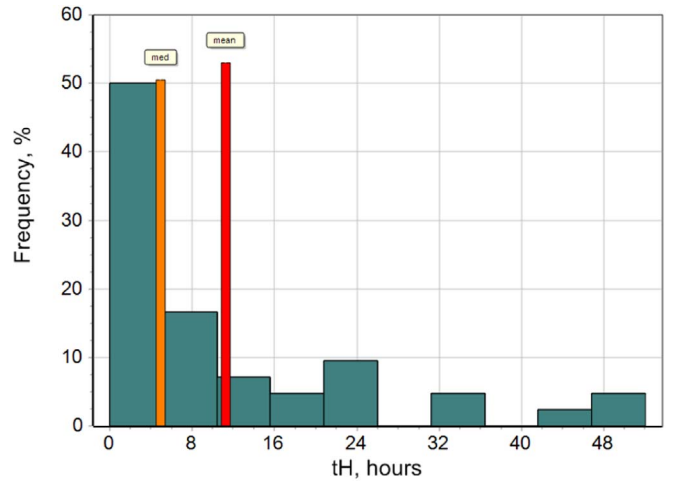
Figure 3. Distribution of the FD events associated with solar parent events situated on the center of the visible solar disk ($-30° \leqslant \Phi_s \leqslant 30°$), with respect to t_H.

3. Event 3 at 2001 January 31 on 08:05 UT.
4. Event 4 at 2003 November 4 on 06:25 UT.

Evidently, due to the small number of events, the results from a possible statistical analysis on this sample would be (the least) doubtful; therefore, it was not pursued further. Furthermore, the second event was also considered unreliable regarding its parent solar identification. Nonetheless, the GCR depressions associated with events that fall in the central part of the visible solar disk are plenty enough. Additionally, in order to increase the probability of FDs that fall under category 3 (see Section 1) and thus explore the effect of the full structure (shock, sheath, ejecta) on the disturbance on GCRs, we limited the central bin to heliolongitudes in the range of $-30° \leqslant \Phi_s \leqslant 30°$, and this sample consists of 42 well-identified FDs. This is because it is expected that these events result from (a) the effects of strong shocks, since those are strongest at the nose and thus the effect of the shock on GCRs is the greatest from central heliolongitudes, and (b) the effect of the ejecta (and/or MC, if present), since during these events the observer (i.e., Earth) is more likely to penetrate well within the ejecta (Cane et al. 1996; Belov et al. 2015). As a result, this is the sample that we will further utilize in this study, and the complete list of the events, summarizing their main characteristics, is presented in full in the Appendix.

3.2. Distribution of t_H and Definition of Subgroups

Figure 3 shows the distribution of t_H for the events that fall in the central part of the visible solar disk (i.e., $-30° \leqslant \Phi_s \leqslant 30°$). As can be seen, the maximum t_H is identified at around 6 hr (median value; depicted with an orange vertical line). This, in turn, means that the maximum of the IMF is observed within 6 hr from the SSC. Based on this distribution, we defined the following ordering of the events and split them into three subgroups:

1. Early—$t_H < 6$ hr [21 events].
2. Medium—$6 \leqslant t_H \leqslant 15$ hr [10 events].
3. Late—$t_H > 15$ hr [11 events].

One should further note that the typical duration of an ICME extends from 22.4 to 32.8 hr, depending on whether an MC was identified (Kilpua et al. 2017). Additionally, assuming that
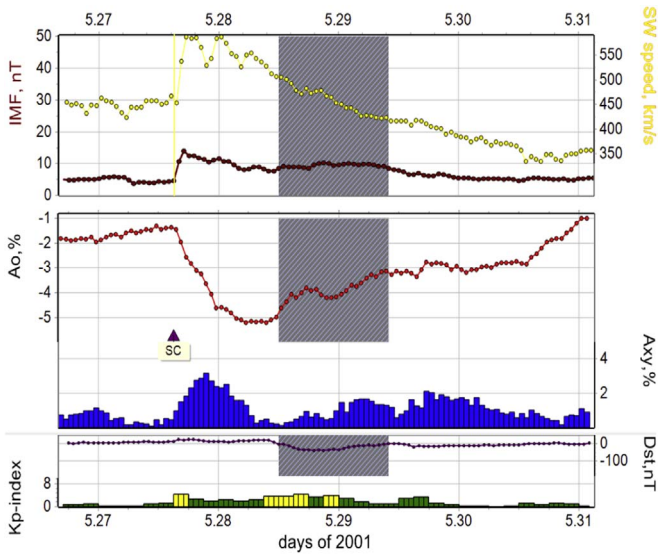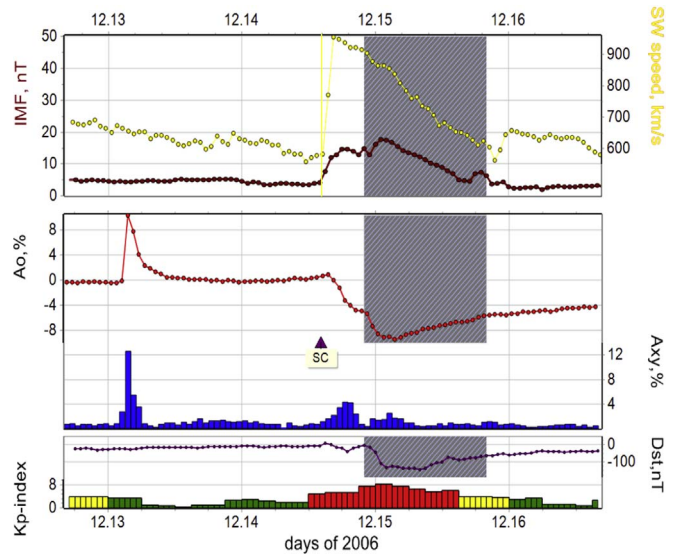
Figure 4. Event on 2001 May 27–29. From top to bottom: the SW speed [km s^{-1}] and the magnitude of the IMF intensity [nT], the variation in the CR density [$A0$, %] and the equatorial component of the CR vector anisotropy [A_{xy}, %], and the evolution of the geomagnetic indices (Dst and Kp). The gray shaded area marks the duration of the MC; the vertical yellow line indicates the timing of the SSC.

Figure 5. Event on 2006 December 13–16. From top to bottom: the SW speed [km s^{-1}] and the magnitude of the IMF intensity [nT], the variation in the CR density [$A0$, %] and the equatorial component of the CR vector anisotropy [A_{xy}, %], and the evolution of the geomagnetic indices (Dst and Kp). The gray shaded area marks the duration of the MC; the vertical green line indicates the timing of the SSC.

a sheath and an ejecta region are present, their intervals are not independent from each other, but the length of the ejecta interval overcomes the sheath by a factor of 3 (Masías-Meza et al. 2016). Therefore, the sheath region should, in principle, occupy a fraction ranging from 5.6 to 8.2 hr, and the ejecta may last from 16.8 to 24.6 hr. Moreover, most recently, the mean duration of the sheath and that of the "magnetized" ejecta were calculated to be 12 and 19.2 hr, respectively (Janvier et al. 2019). Hence, the groups selected in this study (with an independent classification) correspond roughly to the observed duration (or significant fractions thereof) of IP sheaths and ejecta.

In what follows we provide typical examples for each of the three subgroups, defined above.

3.2.1. The Early Group

The Early group of events is represented by the event on 2001 May 27–29 (Figure 4). Figure 4 (from top to bottom) presents the SW speed [in km s^{-1}] and the magnitude of the IMF [in nT], the variation in the CR density [$A0$, %] and the equatorial component of the CR vector anisotropy [A_{xy}, %], and the evolution of the geomagnetic indices (Dst and Kp). The gray shaded area marks the duration of the MC; the vertical yellow line indicates the timing of the SSC and thus the commencement of the FD. As can be seen, in this example the propagating ICME includes a clear MC (Richardson & Cane 2011). However, the IMF magnitude and its corresponding increase within the MC are weak and relatively stable (top panel of Figure 4). The maximum of the IMF ($B_{max} = 13.9$ nT) is observed at the shock front and in close association—in time—with the maximum SW speed ($V_{SW} = 586$ km s^{-1}). Additionally, this interplanetary disturbance leads to a weak geomagnetic perturbation as is demonstrated by Kp (4+) and Dst (−42 nT) indices (bottom panel of Figure 4). At the same time, the corresponding magnitude of the FD (i.e., $A0$) is large (3.9%), and the minimum of the FD is

observed prior to the arrival of the MC, near the leading boundary of the ejecta. Also, the equatorial component of the vector anisotropy ($A_{xy} = 3.18$%) significantly increases, right after the arrival of the SSC (middle panel of Figure 4).

3.2.2. The Medium Group

The Medium group of events is represented by the event on 2006 December 14–16 (Figure 5). This is a large ($A0 = 8.6$%), typical two-step FD. The agent CME was very fast ($V_{CME} = 1774$ km s^{-1}) and was (apart from the FD) also associated with a large ground level enhancement (GLE) that preceded the FD, on 2006 December 13 (GLE70; Mishev & Usoskin 2016), a feature that is also presented in Figure 5 (middle panel).

The maximum IMF intensity ($B_{max} = 17.9$ nT) and the minimum of the GCR depression are in very close agreement and fall within the MC; however, both occur almost 10 hr after the time of maximum SW speed ($V_{SW} = 896$ km s^{-1}; top and middle panels of Figure 5). A very large geomagnetic storm was associated with this CME (e.g., Kp = 8+, Dst = −146 nT; bottom panel of Figure 5), and its most disturbed part falls within the MC. The equatorial component of the vector anisotropy reached the high value of $A_{xymax} = 4.35$% in this event.

3.2.3. The Late Group

The Late group of events is represented by the event on 2000 February 20–22 (Figure 6). As can be seen, the IMF strength in the ICME and, in particular, within the MC is relatively high ($B_{max} = 16.9$ nT) and distinguished compared to the maximum value of the IMF reached in the vicinity of the shock wave (top panel of Figure 6). At the same time, the geomagnetic activity is relatively moderate, as is presented by the indices $Kp_{max} = 5$ and $Dst_{min} = −26$ nT. In addition, this geomagnetic storm has two episodes: one associated with the arrival of the shock
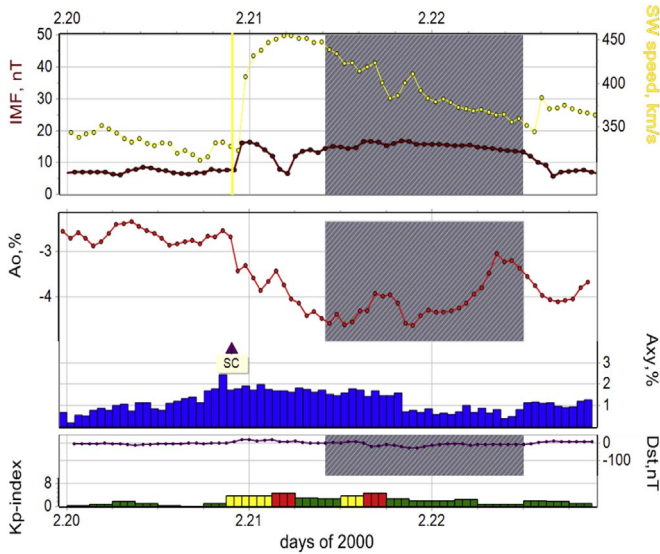
Figure 6. Event on 2000 February 20–22. From top to bottom: the SW speed [km s^{-1}] and the magnitude of the IMF [nT], the variation in the CR density [$A0$, %] and the equatorial component of the CR vector anisotropy [A_{xy}, %], and the evolution of the geomagnetic indices (Dst and Kp). The gray shaded area marks the duration of the MC; the vertical yellow line indicates the timing of the SSC.

wave, and another one associated with the MC (bottom panel of Figure 6). The FD has a total magnitude $A0 = 2.1\%$, and the minimum of the FD is located within the MC. The equatorial component of the vector anisotropy increases before the arrival of the SSC ($A_{xymax} = 2.45\%$) and maintains elevated values for a long time period (i.e., for almost an entire day).

3.3. Studying Subgroups

3.3.1. Superposed Epoch Analysis (SEA)

Here we analyze the average time profiles of the three subgroups, utilizing the SEA as a statistical method in order to determine the averaged time profiles of physical parameters (i.e., $A0$, B_{max}, V_{SW}) obtained in situ. Such an analysis is based on the comparison of various time series for each data set and each subgroup. The basic underlying assumption is that the physical parameters behave in a similar manner, and thus when one averages the time series of all events (in each subgroup) on a normalized timescale, one shall obtain meaningful mean profiles. In our work, the time of the SSC (which denotes the onset of an FD) was used as the key (i.e., zero) time of the SEA, and the corresponding mean time profiles were constructed with a 1 hr step (i.e., utilizing hourly data). Figure 7 depicts the resulted GCR time profile at a fixed energy of 10 GV for each of the subgroups: Early, Medium, and Late (from top to bottom). Within each of the three panels, the averaged Kp index is also presented, along with the averaged distributions of the magnetic field (i.e., IMF, B_{max}) and the SW speed (i.e., V_{SW}), which are depicted as rectangles. Furthermore, the arrows indicate the time of maximum of B and V_{SW}, respectively, for each group. Table 1 presents the outputs of the SEA.

1. In the Early group (Figure 7, top panel), V_{SW}, most often, lags behind the maximum of the IMF B_{max}, while the opposite is true for the Medium and the Late groups

(Figure 7, middle and bottom panels). Moreover, the distribution of the maxima of the V_{SW} in all three subgroups is rather wide; however, the widest one is obtained in the Late group (Figure 7, bottom panel).

2. The largest averaged FD magnitude (i.e., $A0$) is revealed in the Medium group (Figure 7, middle panel) and is ∼5.4%. Such an $A0$ value should be considered as a very large one (Belov et al. 2001) even for a single FD, let alone that the application of the epoch method leads to an underestimation of the maximum size of the FD, due to averaging. In the Early group (Figure 7, top panel), the average value of the FD magnitude is smaller ($A0 = 3.01\%$) compared to the one obtained in the Medium group, and in the Late group (Figure 7, bottom panel) $A0$ is even smaller ($A0 = 2.1\%$).

3. The level of geomagnetic activity—as is depicted by the Kp index—differs in approximately the same way: in the Medium group (Figure 7, middle panel), the average storm reaches a level between moderate and strong (according to NOAA space weather scales[7]). For the Early group (Figure 7, top panel), the average Kp-index maximum is about 5+, while for the Late group (Figure 7, bottom panel), Kp is ∼5. Additionally, in the Medium group, the magnetic storm is not only the largest (in terms of magnitude) but also the longest (in terms of duration) since the storm level (Kp, 5+) lasts almost a day (24 hr), and the disturbed level (Kp ∼ 4) is further observed for more than 2 days from the FD onset. In the other groups, the averaged magnetic storm has a much shorter duration—especially in the Early group the storm ends within only 6 hr. Moreover, in the Late group, the geomagnetic activity has a longer duration (∼10 hr).

One should further note that we do not discuss, in a similar way, the duration of the FDs. This is because the recovery of the CR intensity is much slower than the recovery of Earth's magnetic field, and often there is no time for the FD to end before the start of a new event. Therefore, the $A0$ time profiles in Figure 7, obtained by the superposed method, cannot be used for the accurate identification of the duration of the FDs.

3.3.2. Mean Values

Table 2 presents a summary of the obtained mean values for various parameters of the SW, cosmic rays, and geomagnetic activity for each of the selected subgroups. For each subgroup, n stands for the number of events used in the calculations. In particular, the parameters of the SW employed in the study were as follows:

1. B_{max}—the maximum IMF intensity [nT].
2. V_{SW}—the maximum SW speed in the event [km s^{-1}].
3. $V_{max}B_{max}$—the product of the parameters above divided by the average values of 5 nT and 400 km s^{-1}, respectively.

The geomagnetic activity parameters/indices were as follows:

1. Kp_{max}—the maximum Kp index within the FD event.
2. Ap_{max}—the maximum Ap index within the FD event [2nT].

---

[7] https://www.swpc.noaa.gov/noaa-scales-explanation
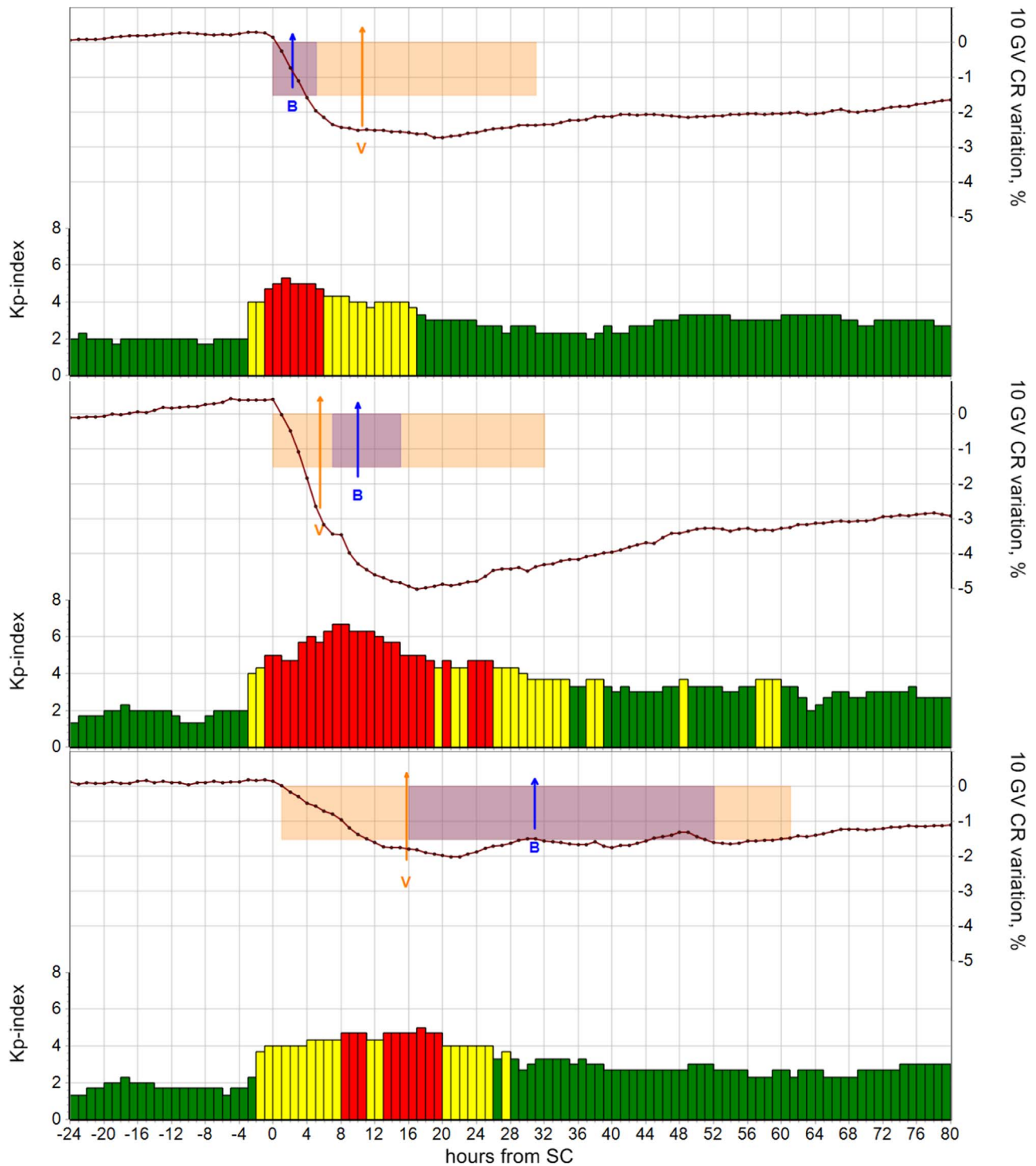
Figure 7. Behavior of averaged CR variations with a rigidity of 10 GV and the Kp index of the geomagnetic activity for different subgroups (Early, Medium, Late—top, middle, and bottom panels, respectively) obtained by the epoch method (zero hour is the hour with SSC). The arrows indicate the average value for each group, and their position on the plot refers to the time of maximum for the IMF intensity and the SW speed, respectively.

3. Dst_{min}—the minimum Dst value within the FD event [nT].

The cosmic-ray parameters and related parameters/products were as follows:

1. $A0$—the magnitude of the FD at a fixed rigidity of 10 GV [%].

2. D_{Min}—the maximum hourly decrease of the CR density in the event [%].

3. $A_{xy_{max}}$—the maximum value of the equatorial component of the CR vector anisotropy [%].

4. $A_{z_{range}}$—the range of the north–south component of the CR vector anisotropy [%].

5. R_{CR}—the critical rigidity [GV] (Belov & Ivanov 1997).

Table 1
Mean Values Resulting from the Application of the SEA

Group	$A0$	Kp	B_{max}	$t_{B_{max}}$	V_{SW}	$t_{V_{max}}$	Time Range of B_{max}	Time Range of V_{SW}
Early	3.01	5+	18.9 ± 8.0	2.29	564.6 ± 98.8	10.5	[0; 5]	[0; 31]
Medium	5.4	7	26.4 ± 15.9	10	634.5 ± 183.7	5.5	[7; 15]	[0; 32]
Late	2.1	5	17.7 ± 5.3	30.9	497.4 ± 85.6	15.7	[16; 52]	[1; 61]

Table 2
Mean Values and Statistical Errors for All Solar Wind, Geomagnetic Index,
Cosmic Ray, and Time Parameters for Each of the Groups: Early, Medium,
and Late

Subgroups	Early, ($n = 21$)	Medium, ($n = 10$)	Late, ($n = 11$)
	($t_H < 6$)	($6 \leqslant t_H \leqslant 15$)	($t_H > 15$)
Mean SW Parameters and Geomagnetic Indices			
B_{max}, (nT)	18.9 ± 1.7	26.4 ± 5.0	17.7 ± 1.6
V_{SW}, (km s^{-1})	564.6 ± 21.6	634.5 ± 58.1	497.4 ± 25.8
$V_{max}B_{max}$	5.5 ± 0.6	9.2 ± 2.4	4.4 ± 0.5
R_{CR}, (GV)	56.1 ± 10.7	116.5 ± 29.6	74.1 ± 19.3
Kp_{max}	5.2 ± 0.3	6.3 ± 0.6	5.6 ± 0.3
Ap_{max}, (2nT)	69.4 ± 11.4	128.7 ± 31.4	74.0 ± 12.1
Dst_{min}, (nT)	-59.7 ± 7.6	-133.9 ± 40.6	-79.6 ± 13.0
Mean Cosmic-Ray Parameters			
$A0$, (%)	3.79 ± 0.55	6.75 ± 0.99	3.30 ± 0.67
D_{Min}	-0.73 ± 0.12	-1.15 ± 0.28	-0.49 ± 0.06
A_{xymax}, (%)	1.99 ± 0.16	2.69 ± 0.32	1.83 ± 0.12
A_{zrange}, (%)	2.13 ± 0.18	2.32 ± 0.23	2.55 ± 0.47
Mean Temporal Scale Parameters			
$t_{V_{SW}}$, (hr)	10.52 ± 1.91	5.50 ± 3.04	15.73 ± 6.20
t_H, (hr)	2.29 ± 0.32	10.00 ± 0.84	30.91 ± 3.96
t_A, (hr)	12.81 ± 2.58	8.50 ± 1.80	19.82 ± 5.36
t_M, (hr)	13.71 ± 2.27	17.70 ± 3.39	20.64 ± 4.73
t_D, (hr)	4.05 ± 1.12	5.30 ± 0.93	13.45 ± 4.13

Moreover, several different time-related parameters were
defined and utilized. Specifically, these are as follows:

1. t_H—the time difference from the onset of the FD event (as
   is denoted by the SSC) to the time of the maximum of
   IMF intensity [hr].
2. $t_{V_{SW}}$—the time difference from the onset of the FD event
   to the time of the maximum of the SW speed [hr].
3. t_M—the time difference from the onset of the FD event to
   the time of the minimum of the CR density [hr].
4. t_D—the time difference from the onset of the FD event to
   the time of the maximum hourly decrease of CR
   density [hr].
5. t_A—the time difference from the onset of the FD event to
   the time of the maximum $A_{xy_{max}}$ [hr].

From Table 2 and Figure 8 it can be seen that the Medium
group is eminently distinguished in almost all parameters
compared to the other two groups (i.e., Early, Late). In
particular, the Medium group has the highest average value in
all the parameters/products related to the SW (i.e., B_{max}, V_{SW},
$V_{max}B_{max}$) and the geomagnetic activity (i.e., Kp_{max}, Ap_{max},
Dst_{min}). Furthermore, this group includes the largest FDs in
terms of magnitude (i.e., $A0$; see Figure 8), with the largest
$A_{xy_{max}}$. There is only one parameter, $A_{z_{range}}$, for which the Late

group (2.55 ± 0.47) overcomes the obtained value for the
Medium group (2.32 ± 0.23). However, this difference is
marginal and lies well within the statistical error.

Our results show that the onset time of the FDs (as is
denoted by the SSC), in all three groups, is marked after the
arrival of the maxima of the SW disturbance (i.e., both t_H and
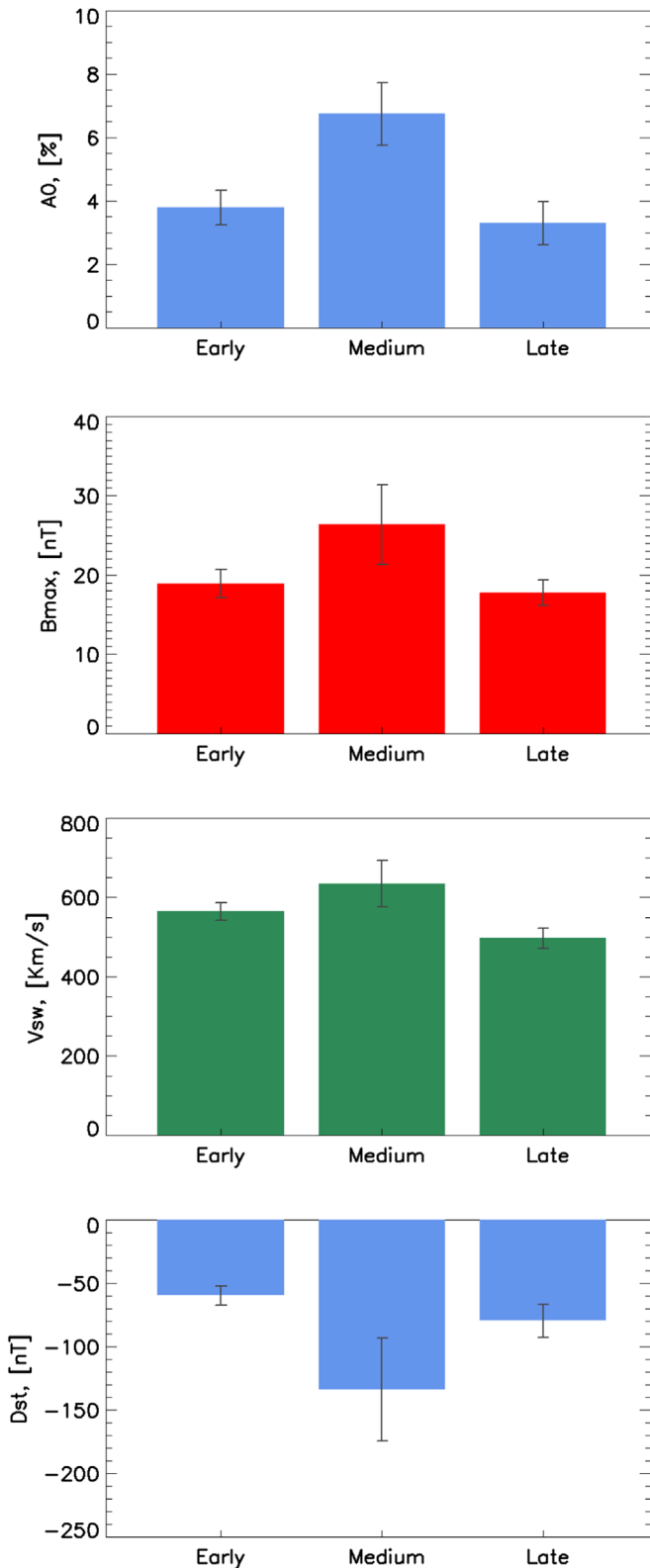$t_{V_{SW}}$ are >0).

3.3.3. Correlation Analysis

We have further searched for correlations of the magnitude
of the FD (i.e., $A0$) to the SW-related parameters for each
subgroup. Figure 9 shows, from top to bottom, the amplitude of
the FD ($A0$, [%]) versus (i) the in situ maximum IMF intensity
(B_{max}), (ii) the in situ maximum SW speed in the event (V_{SW}),
(iii) the product $V_{max}B_{max}$, (iv) the ICME transit speed to 1 au
(V_{trans}),[8] (v) the plane-of-sky speed of the associated agent
CME (V_{CME}), and (vi) the X-ray magnitude of the associated
flare (X_{magn}). Each column in Figure 9 refers to each of the
subgroups of the study, i.e., Early, Medium, and Late,
respectively. The dependence of the magnitude of the FD
(i.e., $A0$) on the maximum IMF intensity (B_{max}) for each of the
three groups is presented in the top row of Figure 9. One can
see that in the Late group B_{max} seems to have an upper limit of
24.6 nT, while the Early group has a similar cutoff at 34.6 nT.
However, the Medium group represents the highest spread of
B_{max} values, spanning from 12.9 up to 55.8 nT. Consequently,
the Medium group seems to have very strong magnetic field
enhancements, more than 2 times higher compared to those
retrieved for the Late group and ∼1.7 times higher compared to
the Early group. As a result, $A0$ for the Medium group is larger
compared to the other two groups with similar factors.
Additionally, it seems that the amplitude of the FD (i.e., $A0$)
is ordered around the product $V_{max}B_{max}$ for both the Early and
Late groups; however, for the Medium group there seems to be
a larger spread. Finally, $A0$ in the Medium group seems to be
better ordered by the V_{SW} and V_{trans}.

In particular, linear regressions of the FD magnitude
(i.e., $A0$) to all the aforementioned parameters were con-
structed. Table 3 provides these regressions. In practice, the
value of the parameter (e.g., magnetic field–B_{max}) returns the
expected value of the $A0$ for each subgroup of events. Column
(1) of Table 4 presents the actual quantity used for the
correlations, Columns (2)–(4) display the relevant Pearsons
correlation coefficient cc and the respective standard error SE_{cc},
which is calculated as $SE_{cc} = \sqrt{1 - cc^2/(n - 2)}$, n being the
number of pairs used for the calculation of cc (Papaioannou
et al. 2016, 2018). This number (n) is included in Table 2 for
every subgroup.

From Table 4 it can be seen that for the Early group of events
the expected magnitude of the FD ($A0$) is highly ($cc = 0.72$)

---

[8] The transit speed (mean velocity of ICME between Sun and Earth) is
determined from the difference of the time between the onset of the CME at the
Sun and the arrival time of the corresponding ICME at Earth (Belov et al.
2014).

Figure 8. Histograms of selected parameters from Table 2. From top to bottom, the panels depict $A0$, B_{max}, V_{SW}, and D_{st} for each of the three subgroups: Early, Medium, and Late. The indicated statistical errors are those presented in Table 2.
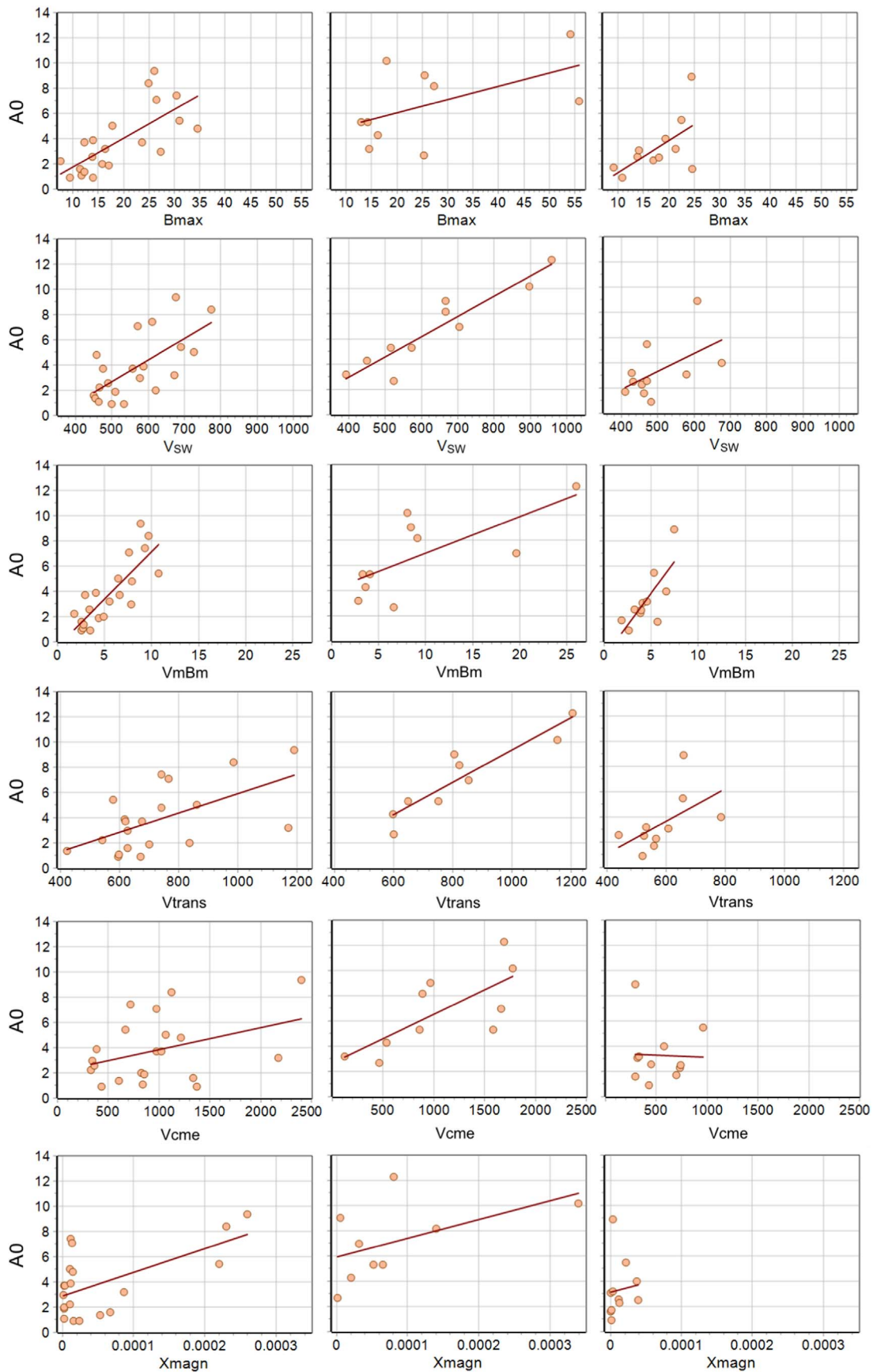
important correlation is obtained between $A0$ and the product $V_{max} B_{max}$. All of the coefficients for each subgroup are significant and highlight the trend that the size of the FD (i.e., $A0$) is influenced by the magnetic field strength and the SW conditions. As was noted in Section 1, the size of FDs is influenced by the magnetic field. This is evident in the significant cc's obtained between $A0$ and B_{max} (at any of the three subgroups) but also by the even stronger correlations of $A0$ to $V_{max} B_{max}$, which is an index that quantifies the disturbed conditions that appear to be due to the distorted magnetic field of the IP medium, resulting from the evolution of ICMEs (Belov et al. 2001). This can also be considered as a proxy for the normalized convective electric field or equivalently as the normalized magnetic flux that passes over the observer (Dumbović et al. 2012). Moreover, fairly significant correlations of the FD magnitude to the maximum SW speed (V_{SW}) and the transit speed of the driving disturbance (V_{trans}) point to the fact that fast ICMEs that propagate into the IP space, from the Sun to 1 au, have less time to fill with GCRs and thus are associated with larger (in terms of magnitude) FDs.

In every subgroup of this study, MCs are prevalent. Specifically, 29% (6/21) in the Early group, 80% (8/10) in the Medium group, and 64% (7/11) in the Late group are FDs driven by ICMEs that were identified with an MC structure.[9] The three largest FDs are marked on 2004 January 22 ($A0 = 8.6\%$), 2005 May 15 ($A0 = 9.5\%$), and 2006 December 14 ($A0 = 8.6\%$) (for a fixed rigidity of 10 GV), all of which are included in the Medium group.

An insignificant anticorrelation of the FD magnitude to the CME speed is found for the events of the Late group. Furthermore, a very weak correlation appears also in the same group of events between $A0$ and the X-ray magnitude of the associated solar flare (Table 4).

Figure 10 presents all FDs in our sample, for each of the three subgroups, Early (red square), Medium (green diamond), and Late (blue triangle), as a function of their amplitude (y-axis: $A0$ [%]) and the position of the FD minimum (x-axis; arbitrary units) within a conceptually ICME shock-sheath-ejecta (including MCs) structure. The shock is denoted with a solid black vertical line, whereas the start and the end of the ejecta are depicted with a pair of dotted vertical lines. One should note that the shock-sheath region is magnetically connected to the ambient IP space and is characterized by disturbed conditions and a highly fluctuating magnetic field ahead of the propagating ejecta, while the ejecta (and/or MC) is not magnetically connected to IP plasma and is further characterized by a smooth magnetic field (Kilpua et al. 2017). As can be seen, all of the FDs of the Medium and Late groups reach their FD minimum within (or at least on the leading boundary of) the ejecta (and/or MC, when present), while the Early group FDs have a strong presence within the sheath region, as well as within the ejecta. This shows that in the majority of the events the shielding of the propagating ICME/ejecta is actually most effective once the peak of the magnetic field (B_{max}) has already passed over the observer for more than 6 hr—as is demonstrated by the FD amplitude ($A0$) for the Medium and Late groups, respectively. At the same time, the fact that 38% of the events of the Early group ($t_H < 6$ hr) reach their FD minimum (i.e., maximum $A0$) within the sheath region, where turbulence and magnetic reconnection are

correlated with B_{max} (especially for the Early group), and at the same time the highest coefficient ($cc = 0.93$) appears in the Medium group and is the output of the correlation of the FD magnitude to V_{SW} and to V_{trans}. For the Late group the most

_____
9   http://www.srl.caltech.edu/ACE/ASC/DATA/level3/icmetable2.htm

Figure 9. Magnitude of the FD ($A0$) vs. (from top to bottom) the maximum IMF intensity B_{max}, the maximum SW speed V_{SW}, the product $V_{max} B_{max}$, the transit speed of the disturbance V_{trans}, the speed of the agent CME V_{CME}, and the magnitude of the associated X-ray flare X_{magn}. Each column (from left to right) corresponds to each of the three subgroups, i.e., Early, Medium, and Late.

Table 3
The Linear Regressions for the Calculation of $A0$ Based on Solar and In Situ Data, for Each Parameter Displayed in Figure 9

Group	Early	Medium	Late
B_{max}	$A0 = -0.506^*B_{max} + 0.227$	$A0 = 3.979^*B_{max} + 0.105$	$A0 = -1.208^*B_{max} + 0.254$
V_{SW}	$A0 = -5.851^*V_{SW} + 0.017$	$A0 = -3.407^*V_{SW} + 0.016$	$A0 = -3.707^*V_{SW} + 0.014$
$V_{max}B_{max}$	$A0 = -0.344^*V_{max}B_{max} + 0.75$	$A0 = 4.116^*V_{max}B_{max} + 0.287$	$A0 = -1.231^*V_{max}B_{max} + 1.02$
V_{trans}	$A0 = -1.731^*V_{trans} + 0.007$	$A0 = -3.424^*V_{trans} + 0.012$	$A0 = -3.957^*V_{trans} + 0.013$
V_{CME}	$A0 = 2.134^*V_{CME} + 0.0017$	$A0 = 2.651^*V_{CME} + 0.0039$	$A0 = 3.522^*V_{CME} -0.0004$
X_{magn}	$A0 = 2.868^*X_{magn} + 1.8759E+04$	$A0 = 5.937^*X_{magn} + 1.4752E+04$	$A0 = 3.110^*X_{magn} + 1.5678E+04$

Table 4
Pearsons Correlation Coefficients (cc) between the Magnitude of the Forbush Decrease ($A0$) and the SW-related Parameters: Maximum IMF Intensity (B_{max}), Maximum SW Speed in the Event (V_{SW}), the Product $V_{max}B_{max}$, and the Correlation Coefficient between B_{max}, V_{SW}, V_{trans}, V_{CME}, and X_{magn} for Each of the Subgroups

	A0		
	Early	Medium	Late
	$cc \pm SE_{cc}$		
B_{max}	**0.72 ± 0.15**	0.53 ± 0.30	0.60 ± 0.27
V_{SW}	**0.67 ± 0.17**	**0.93 ± 0.13**	0.54 ± 0.28
$V_{max}B_{max}$	**0.82 ± 0.13**	**0.70 ± 0.25**	**0.76 ± 0.22**
V_{trans}	**0.59 ± 0.18**	**0.93 ± 0.13**	0.54 ± 0.28
V_{CME}	0.38 ± 0.21	**0.73 ± 0.24**	−0.04 ± 0.33
X_{Magn}	**0.60 ± 0.18**	0.51 ± 0.30	0.10 ± 0.33

Note. The corresponding standard errors SE_{cc} are also presented, where n is the number of pairs used for the calculation of cc and corresponds to those denoted in Table 2 for each subgroup. The most significant coefficients are shown in boldface type.

prevalent, points to their corresponding effect on the diffusion of cosmic rays that lead to observable GCR depressions (Dumbović et al. 2011; Jordan et al. 2011).

4. Discussion

The analysis of the response of GCRs, as this was calculated using the recordings of the worldwide NM network for a fixed rigidity of 10 GV, to the passage of ICMEs and their associated shocks (as denoted in this study by the SSC) indicated the following:

1. Both the shock and the ICME contribute to the modulation of GCRs, which leads to depressions of the CR intensity at Earth from NMs.
2. There were four events that would fall under category 1, i.e., driven only by a shock.
3. The magnitude of the FD ($A0$) is well correlated with the maximum IMF intensity (B_{max}), the maximum SW speed (V_{SW}), and the transit speed of the disturbance (V_{trans}).

Additionally, the t_H parameter, which is the time delay (in hr) from the maximum of the magnetic field strength of the IMF in the FD to the onset of the FD event (as is marked via the SSC), has been introduced and used in this work. As a result, three subgroups of events were identified on the basis of t_H: Early ($t_H < 6$ hr), Medium ($6 \leqslant t_H \leqslant 15$ hr), and Late ($t_H > 15$ hr). For each subgroup we further investigated the mean characteristics of the SW, geomagnetic indices, and cosmic-ray parameters (Table 4). The comparison of the three subgroups showed that the Medium group

1. encompasses the highest values for all parameters investigated;
2. involves the largest FDs in terms of magnitude ($A0$) and equatorial component anisotropy (A_{xymax});
3. has the strongest magnetic field (B_{max});
4. has the highest SW speed (V_{SW}); and
5. incorporates most of the two-step FDs.[10]

One should note that ICMEs present a variety of often complex and not idealized magnetic configurations, stemming from the evolution of the ICME during the crossing of the observer, as well as the internal magnetic field configuration (Nieves-Chinchilla et al. 2018). Therefore, it is expected that the t_H parameter will depend on such complexity. Moreover, t_H is also dependent on the polarity of MCs (when present), which has been shown to drive their geoeffectivity and consequently the presence (or not) of SSCs (Kilpua et al. 2012). However, it is beyond the scope of this work to investigate these aspects further. Nonetheless, such studies appear as natural future steps.

Moreover, the resulting correlation coefficients per subgroup highlighted the strong relation between the magnitude of the FD ($A0$) and the parameters that describe the IP conditions (B_{max}, V_{SW}, $V_{max}B_{max}$). At the same time, it was shown that for the Medium group of FD events the magnitude ($A0$) is significantly correlated with V_{CME}, V_{trans}, and V_{SW}. Such high correlations point to the fact that fast CMEs/ICMEs for which t_H falls within [6, 15] hr lead to larger FDs. At the same time, the insignificant correlations (and anticorrelations) of $A0$ with the characteristics of their parent solar events (i.e., magnitude of the associated flare and CME speed) for the Late group can most probably be attributed to the fact that such long-lasting (in terms of duration) FDs usually involve more than one agent solar event that masks the one-to-one association. Such results are in very good agreement with previous studies that aimed at unraveling the effect of ICMEs on the short-term modulation of GCRs, i.e., FDs (Cane 2000; Belov 2009; Richardson & Cane 2010, 2011).

The timing of the FD minimum (i.e., when the maximum $A0$ is reached) is governed by the propagation characteristics of the disturbance, and the obtained amplitude (i.e., $A0$) is well determined by the magnetic field strength, in all three subgroups of FD events, with the higher correlation identified between $A0$ and B_{max} for the Early group ($cc = 0.72$). In contrast, the relevant FD timing (i.e., FD minimum) and amplitude ($A0$) for the Medium group is highly correlated with V_{SW}, V_{trans}, and V_{CME}. Parker (1965) presented the transport equation of cosmic rays in the heliosphere, including contributions from four basic physical effects: (a) diffusion, (b) drift, (c) convection, and (d) energy change (Jokipii 1971). Our results imply that the last two contributions, which are directly related to the SW speed and the propagation

---

[10] From the events utilized in this study.
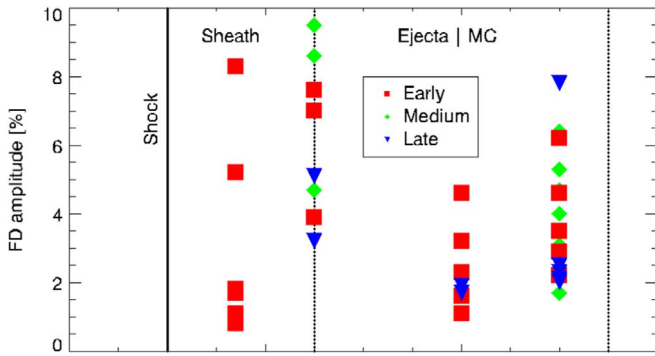
Figure 10. Representation of all FDs in our sample for each of the three subgroups, Early, Medium, and Late (see label in the plot), as a function of $A0$ (y-axis) and the position of the FD minimum (i.e., $A0$ maximum) within the ideal ICME characterized by a shock-sheath-ejecta structure (in arbitrary units; x-axis).

conditions, are prevalent for the FDs of the Medium group (see Table 4 and Figure 10), showing that the shielding from the (at least partially) closed magnetic field lines of the magnetized ejecta is the primer agent. However, this does not mean that the preceding turbulent shock-sheath region does not contribute to these FDs—as is highlighted by the presence of two-step FDs in this subgroup (Barnden 1973). Additionally, the enhanced magnetic field and the consequent depletion of GCRs, which lead to reduced curvature and gradient drifts and exclusion due to fluctuations, reduce the diffusion mean free path (Wibberenz et al. 1998). This mechanism seems to be prevalent in almost half of the cases of the Early group, and given the high correlation of all subgroups to B_{max}, it is certainly in effect in all other subgroups. In turn, this signifies the importance of the turbulent shock-sheath region to short-term GCR depressions (Dumbović et al. 2011). These results are in agreement with theoretical expectations (Le Roux & Potgieter 1991; Wibberenz et al. 1998; Dumbović et al. 2018).

Finally, SEA was applied for each subgroup and was used in order to construct an average time profile of the resulting FDs during the passage of ICMEs (including shock, sheath, and ejecta/MC). Additionally, mean values for 16 different quantities (Table 2)—several of which were observed in situ (i.e., B_{max}, V_{SW}, $D_{st_{min}}$)—were calculated. As a result, it was possible to identify similarities between events in the respective groups and to proceed with comparisons. In particular, significant differences appear in the obtained parameters of the different groups. For example, in the Early group (top panel of Figure 7) B (denoted by the vertical arrow) is peaked toward the start of the FD event, whereas in the Medium group (middle panel of Figure 7) B peaks closer to the obtained FD minimum (i.e., maximum $A0$), and in the Late group (bottom panel of Figure 7) B peaks closer to the recovery of the FD. Additionally, the strongest B belongs to the Medium group, followed by the mean B_{max} values of the Early and Late groups, respectively (see Table 4). Concerning the SW speed V_{SW}, it peaks closer to the start of the FD in the Medium group and closer to the FD minimum in the Early and Late groups, with a larger spread denoted in the latter one. At the same time, V_{SW} is higher in the Medium group, followed by the Early and Late groups (Table 4). Additionally, slower ICMEs are identified in the Late group, whereas the fastest are present in the Medium and Early groups. These results imply that the fast ICMEs of the Medium and Early groups overtake the underlying SW, leading to the compression of the shock-sheath region. However, the Late

group of FDs is associated with slow CMEs and weak flares (see Figure 9, bottom two panels on the right-hand side), and thus such FDs are driven by slow ICMEs. As is known, ICMEs that produce FDs suffer deceleration, whereas the ICMEs that do not produce FDs are accelerated (see Belov et al. 2014, Figure 7). Comparing the average V_{CME} and the average V_{SW} in the corresponding near-Earth disturbance for each subgroup, it seems that the deceleration is most effective in the Early group (a factor of $\sim$2.38), followed by the Medium group (a factor of $\sim$1.73) and the Late group (a factor of $\sim$1.42). The SEA showed that the strongest decrease, in terms of amplitude ($A0$), is obtained for the Medium group, followed by the Early and Late groups—with $A0$ being larger for faster-propagating ICMEs and largest when t_H falls within [6, 15] hr.

5. Summary

The detailed analysis of the FD events and the comparison of their characteristics to their associated ICMEs and their agent solar events (e.g., CMEs) based on the grouping, furnished above, allow us to conclude that (1) the Medium group (when t_H falls within [6, 15] hr) predominates all other groups in terms of FD magnitude ($A0$), pointing to the fact that both the shock sheath and the ejecta are necessary for such deep GCR depressions; (2) $A0$ is larger for faster-propagating ICMEs; (3) the B_{max} of the propagating disturbance is well correlated with $A0$ in all groups, signifying the importance of the turbulent shock-sheath region across selections; and (4) empirical relations connecting $A0$ to SW properties have been established and presented.

Our results can be effectively used to underpin the effect of large-scale traveling disturbances in the SW that lead to significant GCR short-term depressions, i.e., FDs. Although it has been almost 60 yr since the discovery of this phenomenon, and >20 yr since the continuous monitoring of the Sun with coronagraphs, through the regular *SOHO*/LASCO measurements, FDs still remain unexploited. Given the significant number of space missions that register GCRs at a range of heliospheric distances, understanding FDs and quantifying the relation of their characteristics to those of their agent solar events—as done in this work—provides an opportunity to unravel the effect of ICMEs as they propagate outward into the heliosphere.

Appendix

The 42 Forbush decreases used in this study are listed in Table 5.

Table 5
List of the 42 Forbush Decreases Used in This Study

No.	Date	Time	A_0	Kp_{max}	Ap_{max}	Dst_{min}	B_{max}	V_{SW}	A_{xy}	A_z	Solar Flare				Group
			(%)		(2nT)	(nT)	(nT)	(km s^{-1})	(%)	(%)	Magnitude	Date	Peak Time	Longitude	
1	1997 May 15	01:59:00	1.7	6.7	111	−115	25.3	524	1.6	2.07	C1.3/	1997 May 12	04:42:00	8	M
2	1997 Oct 1	00:59:00	2.2	7	132	−98	13.8	490	2.18	2.25	None	None	None	−10[a]	E
3	1998 Jan 28	17:00:00	1.9	4.3	32	−72	9.1	409	1.52	5.23	C1.1/SF	1998 Jan 25	14:29:00	−25	L
4	1998 Nov 13	01:43:00	2.3	6	80	−133	21.3	428	1.88	5.29	C3.4/	1998 Nov 9	19:39:00	10	L
5	1998 Nov 30	05:07:00	1.1	4.3	32	−23	14	499	1.48	1.76	M1.6/	1998 Nov 27	07:21:00	−9	E
6	1999 Mar 10	01:30:00	0.8	6.3	94	−78	11.7	463	1.34	1.24	C2.9/SF	1999 Mar 7	03:54:00	3	E
7	1999 Apr 16	11:25:00	2.3	7.3	154	−105	24.6	462	1.51	1.34	B4.0/	None	None	0[a]	L
8	1999 Jul 26	23:23:00	2.3	2.3	9	−22	7.5	466	1.69	1	M1.1/2F	1999 Jul 23	18:32:00	−4	E
9	1999 Dec 26	21:30:00	0.9	3.3	18	−29	12.2	454	1.26	1.65	M5.3/1B	1999 Dec 22	18:52:00	−19	E
10	2000 Jan 22	00:23:00	1.7	6.3	94	−97	18.1	431	1.66	1.76	M3.9/1N	2000 Jan 18	17:07:00	−11	L
11	2000 Feb 20	21:39:00	2.1	4.7	39	−26	16.9	455	2.45	1.98	M1.3/2N	2000 Feb 17	20:17:00	−7	L
12	2000 Jun 8	09:10:00	7.6	7	132	−90	24.9	774	3	2.22	X2.3/	2000 Jun 6	14:58:00	−18	E
13	2000 Sep 4	13:33:00	0.7	5.7	67	−36	10.8	482	1.46	1.42	C1.6/SF	2000 Sep 1	05:26:00	18	L
14	2000 Sep 6	17:01:00	1.8	4	27	−33	17.1	509	2.51	2.25	C2.0/SF	2000 Sep 4	05:40:00	14	E
15	2000 Nov 6	09:47:00	7.8	7	132	−159	24.5	609	2.32	4.18	C3.2/SF	2000 Nov 3	18:35:00	2	L
16	2001 Mar 3	11:21:00	2	5	48	−73	14.1	579	2.03	1.83	B6.0/	2001 Feb 28	15:00:00	5	L
17	2001 May 27	14:59:00	3.9	4.3	32	−42	13.9	586	3.18	2.69	M1.2/1N	2001 May 24	19:30:00	−29	E
18	2001 Sep 25	20:25:00	8.3	7.3	154	−102	26.1	677	1.84	4.51	X2.6/2B	2001 Sep 24	09:32:00	−23	E
19	2001 Oct 11	17:01:00	7	6	80	−71	26.5	571	3.81	2.5	M1.4/2F	2001 Oct 9	10:46:00	−8	E
20	2001 Oct 25	08:50:00	1.7	3	15	−42	11.4	449	2.21	1.48	M6.7/2N	2001 Oct 22	14:27:00	−18	E
21	2002 Mar 18	13:22:00	5.1	5.3	56	−37	22.5	469	1.31	1.52	M2.2/1F	2002 Mar 15	22:09:00	3	L
22	2002 Apr 17	11:07:00	6.2	7.3	154	−127	30.4	611	3.01	2.37	M1.2/1N	2002 Apr 15	03:05:00	1	E
23	2002 Aug 18	18:46:00	4.7	5.3	56	−71	14.3	573	2.5	2.5	M5.2/2N	2002 Aug 16	11:32:00	−20	M
24	2003 Nov 20	08:03:00	4.7	8.7	300	−422	55.8	703	2.65	3.09	M3.2/2N	2003 Nov 18	07:23:00	−18	M
25	2004 Jan 22	01:37:00	8.6	7	132	−149	25.4	666	4.32	2.29	C5.5/	2004 Jan 19	22:02:00	9	M
26	2004 Apr 9	02:33:00	1.1	4.7	39	−35	9.4	533	1.17	1.19	M2.4/	2004 Apr 6	12:30:00	−15	E
27	2004 Dec 5	07:46:00	4.6	4.3	32	−58	34.6	457	1.68	1.78	M1.5/SX	2004 Dec 2	23:44:00	2	E
28	2005 May 15	02:38:00	9.5	8.3	236	−263	54.2	959	2.53	3.68	M8.0/SX	2005 May 13	16:13:00	−11	M
29	2006 Dec 14	14:14:00	8.6	8.3	236	−146	17.9	896	4.35	2.07	X3.4/4B	2006 Dec 13	02:14:00	23	M
30	2011 Feb 18	01:30:00	5.2	5	48	−30	31	691	1.55	1.77	X2.2/	2011 Feb 15	01:44:00	17	E
31	2011 Mar 29	16:30:00	3.1	3.3	18	−2	14.5	391	1.4	1.72	None	None	None	−28[b]	M
32	2011 Jun 4	20:44:00	3.5	6.3	94	−39	23.6	556	1.78	1.12	C3.7/	2011 Jun 2	07:22:00	−25	E
33	2011 Oct 5	07:36:00	2.5	4.3	32	−42	13.8	470	1.77	1.94	M1.2/	2011 Oct 1	08:56:00	4	L
34	2012 Jan 24	15:03:00	3.2	4.3	32	−80	16.4	673	1.59	3.02	M8.7/	2012 Jan 23	03:38:00	25	E
35	2012 Jul 14	18:09:00	6.4	7	132	−133	27.3	667	2.62	2.73	X1.4/	2012 Jul 12	15:37:00	15	M
36	2013 Mar 15	05:26:00	1.6	3.7	22	−25	12.2	475	1.58	1.64	C2.0/1F	2013 Mar 12	10:17:00	−1	E
37	2013 Mar 17	05:59:00	4.6	6.7	111	−132	17.8	725	1.72	3.39	M1.1/1F	2013 Mar 15	05:46:00	−12	E
38	2013 Apr 13	22:54:00	5.3	3.3	18	−16	12.9	516	2.98	2.07	M6.5/3B	2013 Apr 11	06:55:00	−12	M
39	2014 Feb 15	13:16:00	4	5	48	−22	16.2	450	1.96	0.99	M2.1/	2014 Feb 12	15:41:00	4	M
40	2015 Sep 20	06:03:00	0.8	7	132	−75	15.8	621	1.15	2.23	C2.6/SF	2015 Sep 18	04:22:00	10	E
41	2015 Nov 6	18:18:00	3.2	6	80	−96	19.4	677	2.23	1.54	M3.7/2B	2015 Nov 4	13:31:00	4	L
42	2016 Jul 19	23:51:00	2.9	5	−1	−23	27.3	576	2.03	2.7	C1.4/SF	2016 Jul 17	05:36:00	−15	E

Notes.
[a] Taken from Gopalswamy et al. (2009a).
[b] For this event we associate a post-eruptive C1.0 flare (S11E28) at 16:47 UT (2011 March 25).
Column (1): event number. Columns (2) and (3): date and time of the SSC (i.e., start time of the FD). Column (4): FD magnitude A_0 (%). Column (5): Kp_{max}. Column (6): Ap_{max} (2nT). Column (7): Dst_{min} (nT). Column (8): B_{max} (nT). Column (9): V_{SW} (km s^{-1}). Column (10): A_{xy} (%). Column (11): A_z (%). Column (12): flare magnitude. Columns (13), (14), and (15): date, peak time, and longitude of the flare. Column (16): subgroup

ORCID iDs

Athanasios Papaioannou ⓘ https://orcid.org/0000-0002-9479-8644
Anatoly Belov ⓘ https://orcid.org/0000-0002-1834-3285
Maria Abunina ⓘ https://orcid.org/0000-0002-2152-6541
Eugenia Eroshenko ⓘ https://orcid.org/0000-0003-3308-993X
Artem Abunin ⓘ https://orcid.org/0000-0003-1427-3045
Anastasios Anastasiadis ⓘ https://orcid.org/0000-0002-5162-8821
Spiros Patsourakos ⓘ https://orcid.org/0000-0003-3345-9697
Helen Mavromichalaki ⓘ https://orcid.org/0000-0002-2595-4754

References

Abunin, A. A., Abunina, M. A., Belov, A. V., et al. 2012, Ge&Ae, 52, 292
Abunina, M. A., Abunin, A. A., Belov, A. V., et al. 2013, Ge&Ae, 53, 10
Arge, C. N., & Pizzo, V. J. 2000, JGR, 105, 10465
Asipenka, A. S., Belov, A. V., Eroshenko, E. A., et al. 2009, AdSpR, 43, 708
Badruddin, K. A. 2016, SoPh, 291, 559
Barnden, L. 1973, Proc. ICRC (Denver), 2, 1277
Belov, A., Abunin, A., Abunina, M., et al. 2014, SoPh, 289, 3949
Belov, A., Abunin, A., Abunina, M., et al. 2015, SoPh, 290, 1429
Belov, A., Eroshenko, E., Yanke, V., et al. 2018, SoPh, 293, 68
Belov, A., & Ivanov, K. 1997, Proc. ICRC (Durban), 1, 421
Belov, A. V. 2009, in IAU Symp. 257, Universal Heliophysical Processes, ed. N. Gopalswamy & D. F. Webb (Cambridge: Cambridge Univ. Press), 439
Belov, A. V., Dorman, L. I., Eroshenko, E. A., et al. 1976, Ge&Ae, 16, 761
Belov, A. V., Eroshenko, E. A., Oleneva, V. A., Struminsky, A. B., & Yanke, V. G. 2001, AdSpR, 27, 625
Brueckner, G. E., Howard, R. A., Koomen, M. J., et al. 1995, SoPh, 162, 357
Burlaga, L. F., Klein, L., Sheeley, N. R. J., et al. 1982, GeoRL, 9, 1317
Burlaga, L. F. E. 1991, in Physics of the Inner Heliosphere II. Particles, Waves and Turbulence ed. R. Schwenn & E. Marsch (Berlin: Springer), 1
Cane, H. V. 2000, SSRv, 93, 55
Cane, H. V., Richardson, I. G., & von Rosenvinge, T. T. 1996, JGR, 101, 21561
Dumbović, M., Heber, B., Vršnak, B., Temmer, M., & Kirin, A. 2018, ApJ, 860, 71
Dumbović, M., Vršnak, B., Čalogović, J., & Karlica, M. 2011, A&A, 531, A91
Dumbović, M., Vršnak, B., Čalogović, J., & Župan, R. 2012, A&A, 538, A28
Forbush, S. 1938, TeMAE, 43, 203
Forsyth, R. J., Bothmer, V., Cid, C., et al. 2006, SSRv, 123, 383
Freiherr von Forstner, J. L., Guo, J., Wimmer-Schweingruber, R. F., et al. 2018, JGRA, 123, 39
Gopalswamy, N., Akiyama, S., Yashiro, S., Michalek, G., & Lepping, R. P. 2008, JASTP, 70, 245
Gopalswamy, N., Akiyama, S., Yashiro, S., Michalek, G., & Lepping, R. P. 2009a, JASTP, 71, 1005
Gopalswamy, N., Yashiro, S., Michalek, G., et al. 2009b, EM&P, 104, 295
Guo, J., Lillis, R., Wimmer-Schweingruber, R. F., et al. 2018, A&A, 611, A79
Howard, R. A., Moses, J. D., Vourlidas, A., et al. 2008, SSRv, 136, 67
Janvier, M., Winslow, R. M., Good, S., et al. 2019, JGRA, 124, 812
Jokipii, J. R. 1971, RvGSP, 9, 27
Jordan, A. P., Spence, H. E., Blake, J. B., & Shaul, D. N. A. 2011, JGRA, 116, A11103
Kilpua, E., Koskinen, H. E. J., & Pulkkinen, T. I. 2017, LRSP, 14, 5
Kilpua, E. K. J., Li, Y., Luhmann, J. G., Jian, L. K., & Russell, C. T. 2012, AnGeo, 30, 1037
Krittinatham, W., & Ruffolo, D. 2009, ApJ, 704, 831
Le Roux, J. A., & Potgieter, M. S. 1991, A&A, 243, 531
Lemen, J. R., Title, A. M., Akin, D. J., et al. 2012, SoPh, 275, 17
Lepping, R. P., Berdichevsky, D. B., Szabo, A., Arqueros, C., & Lazarus, A. J. 2003, SoPh, 212, 425
Lockwood, J. A. 1971, SSRv, 12, 658
Lugaz, N., & Farrugia, C. J. 2014, GeoRL, 41, 769
Masías-Meza, J. J., Dasso, S., Démoulin, P., Rodriguez, L., & Janvier, M. 2016, A&A, 592, A118
McComas, D. J., Bame, S. J., Barker, P., et al. 1998, SSRv, 86, 563
Michalek, G., Gopalswamy, N., Lara, A., & Yashiro, S. 2006, SpWea, 4, S10003
Mishev, A., & Usoskin, I. 2016, SoPh, 291, 1225
Nieves-Chinchilla, T., Vourlidas, A., Raymond, J. C., et al. 2018, SoPh, 293, 25
Papaioannou, A., Anastasiadis, A., Sand berg, I., & Jiggens, P. 2018, JSWSC, 8, A37
Papaioannou, A., Belov, A., Abunina, M., et al. 2019, SoPh, 294, 66
Papaioannou, A., Malandraki, O., Belov, A., et al. 2010, SoPh, 266, 181
Papaioannou, A., Sandberg, I., Anastasiadis, A., et al. 2016, JSWSC, 6, A42
Parker, E. N. 1965, SSRv, 4, 666
Patsourakos, S., Georgoulis, M. K., Vourlidas, A., et al. 2016, ApJ, 817, 14
Richardson, I. G., & Cane, H. V. 2010, SoPh, 264, 189
Richardson, I. G., & Cane, H. V. 2011, SoPh, 270, 609
Schwenn, R., Raymond, J. C., Alexander, D., et al. 2006, SSRv, 123, 127
Wibberenz, G., Le Roux, J. A., Potgieter, M. S., & Bieber, J. W. 1998, SSRv, 83, 309
Winslow, R. M., Schwadron, N. A., Lugaz, N., et al. 2018, ApJ, 856, 139
Witasse, O., Sánchez-Cano, B., Mays, M. L., et al. 2017, JGRA, 122, 7865